”Brush model” for the analysis of flat belt transmissions in steady-state conditions

F. Frendo*, F. Bucchi

Department of Civil and Industrial Engineering, University of Pisa, Largo Lucio Lazzarino, 56122 Pisa, Italy

Abstract

In the present work a novel mathematical model for the analysis of the contact actions between belt and pulleys, particularly suited for flat reinforced rubber belt, is presented. The model considers the tension member, composed of the reinforcement fibers, inextensible and the rubber matrix, which transmits power, as a continuum bed of elastically deformable bristles, fixed to the tension member on one side and in contact with the pulley on the other side. The deformation of the matrix is inversely proportional to the bending stiffness of the bristles, while friction conditions determine the local adhesion/sliding behavior between belt and pulleys. The proposed model can give a detailed description of the contact conditions along the whole contact arc and is able to describe the stick–slip phenomenon which has been experimentally observed by some authors. The model assesses also the power losses due to the contact stresses and to the elastic deformation of the matrix. The results of the model are discussed in comparison with results from classical models, *Grashof* and *Firbank* models, available in the technical literature.

Keywords: belt transmissions, flat belt, rubber belt, mathematical model, contact conditions, power losses, brush model.

1. Introduction

The mechanics of belt drives represents a classic topic of power transmissions, treated in engineering courses and studied by various authors since about two centuries. With reference to flat belt systems, in the literature there are two main models, starting from which many studies and many variants have been developed: these are the *creep model*, often called *Euler* or *Grashof* model, which considers the perfect adhesion of the belt along the arc of adhesion and creep of the belt along the sliding arc, and the *shear and creep model*, also known as *Firbank* model, which considers shear deformation between the belt along the arc of adhesion and creep along the creeping arc.

The first model was initially developed for flat belts, made of leather or textile material, even if it is also used for the case of belts made of a rubber matrix and reinforcing fibers. *Euler* was the first to formulate a relationship, which links the tension of a rope entering and leaving a pulley to the friction between the rope/belt and the pulley, in 1762. This model was reconsidered in 1875 by *Reynolds* who included the speed losses due to belt deformation and in 1883 by *Grashof* which included the effects of the centrifugal force acting on the belt.
Recently, many variations of the creep model have been proposed, including the effects of inertia in the tangential direction of the belt [1], the bending stiffness of the belt [2]–[3], multi-pulley systems [3]–[4], belts with trapezoidal cross-section [5]–[6]. Regardless of the number of simplifying hypotheses, all creep models divide the winding arc into two regiones: an adhesion arc, at the pulley entrance, and a sliding arc toward the exit from the pulley. In the adhesion zone, there is no variation in the tension of the belt and there are no tangential actions between the belt and the pulley. On the contrary, along the sliding arc micro-sliding (micro-slip or creep) occurs between the belt and the pulley, due to a variation in the belt tension, which is a consequence of tangential stresses related to friction. In [7] the creep model was also considered in the case of a variable friction coefficient along the sliding arc as a function of the relative speed between the belt and the pulley.
In all these models, the extension of the adhesion and sliding arcs is simply obtained starting from the knowledge of the relationship giving the belt tension along the sliding arc and from the knowledge of the belt tension in the tight and slack side, which, in turn, is a function of the belt pre–load and of the transmitted torque.

In 1970, *Firbank* [8] proposed a model capable of taking into account the variation in belt tension that occurs along the adhesion arc, due to the angular deformation (shear) of the belt caused by the speed difference between belt and pulley; along the sliding arc the hypotheses remain those of the creep model. This model has been proposed after that rubber belts reinforced in the axial direction were introduced. The model was then discussed and used by other authors [2], [5], [9], also for estimating the transmission efficiency [10]. As already discussed for the creep model, also in the *Firbank* model the extension of the arc along which shear occurs and of the one along which creep occurs is obtained to satisfy the variation of the belt ten-

*Corresponding author. Tel.: +39(0)502218074
E-mail address: francesco.frendo@unipi.it

sion along the whole contact arc.

In [11] the *Firbank* model with elastically deformable belt was used to analyse the steady–state dynamic problem of a system composed of a flat belt and two pulleys. In this case, given the belt pre–load and the speed of the driving pulley, the speed of the belt and the speed of the driven pulley are obtained by an iterative way in order to verify the desired transmitted torque. This approach allows to determine the extension of the arc along which shear occurs on the basis of a phenomenological contact model, considering the static friction limit between belt and pulleys; the total efficiency of the transmission is also estimated by the model.

Della Pietra and *Timpone* made some experimental measurements of the belt tension by using electric strain gauges bonded on the external belt surface in [12]. In their work it is confirmed that the belt tension varies along the whole contact arc. In addition the *stick–slip* phenomenon is observed by the authors on both pulleys. Stick and slip is also mentioned in [13], where the normal and tangential forces acting on the pulleys are measured by force transducers for the case of an abrasive belt.

To the best of the authors' knowledge, *stick–slip* behaviour has not been envisaged by any theoretical models available in the technical literature.

In this paper a mathematical model is presented, inspired to the "brush model" sometimes used for pneumatic tires [14]–[15], capable of accurately describe the belt tension variation and the tangential actions between the belt and the pulley along the whole contact arc. The underlying idea was to use a physically based model to obtain a precise description of the belt behaviour, together with a more in depth analysis of the friction conditions, with the possibility of static–to–dynamic repeated transitions (i.e. *stick–slip*), as experimentally observed by some authors. The model is developed here for the case of axially rigid flat belts with purely elastic behavior of the bristles, which are assumed to have no mass and no damping.

The model is intended to find a solution to the problem of a belt transmission in which the resistant torque is assigned together with the rotating speed of the driving pulley. This, in facts, represents a typical real application.
The solution to this problem, if it exists, is represented by the speed of the belt and the rotating speed of the driven pulley. The problem has to be faced with by a constitutive model of the belt, a contact model between bristles and pulleys and by considering proper congruence and equilibrium conditions.
If the solution is found, the detailed knowledge of the contact actions can also provide an estimate of the power losses related to the contact between belt and pulleys and to the elastic deformation of the belt (see e.g. [16]).

2. Brush model of the belt and contact stresses between belt and pulleys

The basic idea of the brush model is to consider the belt as composed of the tension member, made of the reinforcement fibers, and by the rubber matrix which has to transfer the contact forces between the belt and the pulleys. In this model the

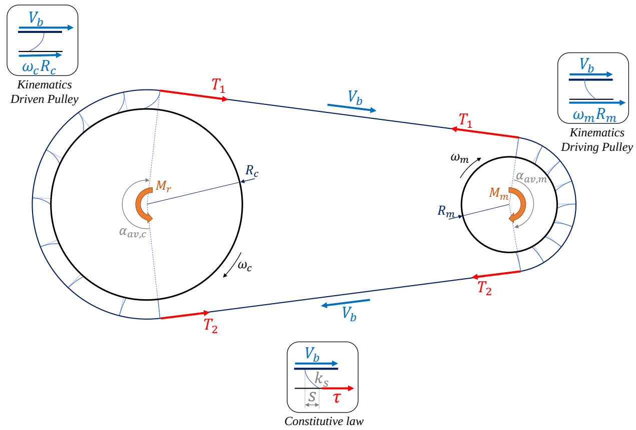

Figure 1: representation of a belt transmission and of the brush model for contact actions

tension member is assumed to be inextensible, while the rubber matrix is assumed to be composed of a bed of elastically deformable bristles, which are constrained to the tension member on one end and in contact with the pulley on the other end. Figure 1 shows a transmission, in which the driving and the driven pulleys have radius R_{dg} and R_{dn}, rotate at ω_{dg} and ω_{dn} and are subjected to the torques M_{dg} and M_{dn}, respectively.

For simplicity, in this model, each bristle is considered as an ideally elastic element, having negligible thickness (compared to the pulley radius), no mass, and no damping associated to it. For this, its deformation occurs instantaneously (there is no transient response). A linear relationship between the contact stress τ and the bristle deformation s is assumed as follows:

$$\tau = k_{\mathrm{s}}\, s \tag{1}$$

where the constant k_{s} can be determined by experiments or by numerical (e.g. finite element) simulation.

According to the previous hypotheses, considering that the tension member is inextensible, its tangential speed is the same in every position and constant over time (steady-state analysis); this speed will be named as V_{b} in the following.

Starting from the entrance into the pulley, the belt (each bristle) deforms due to the difference between the speed of the tension member and the peripheral speed of the pulley; in the first part of the contact arc the bristle keeps in contact to the pulley external surface, until the limit condition imposed by static friction is satisfied:

$$\tau \leq \tau_{\mathrm{s}} = \mu_{\mathrm{s}}\, p \tag{2}$$

where p is the normal pressure, which is given by the well known relationship (based on radial equilibrium of a belt element):

$$p(\alpha) = \frac{T(\alpha) - qV_{\mathrm{b}}^2}{R_i} \tag{3}$$

where α is the angular coordinate, measured starting from the entrance into the pulley, the second term on the numerator represents the inertia load, q is the mass per unit length of the belt and R_i is the radius of the considered pulley (i.e. R_{dg} or R_{dn} for driving or driven pulley, respectively).

A discontinuous coulomb friction model, with coefficient μ_{s} and $\mu_{\mathrm{d}} \leq \mu_{\mathrm{s}}$ is assumed. Then, the contact arc consists of an initial adhesion arc, in which the bristles deform due to different speed of the belt and the pulley and that extends till Eq. 2 is valid. Once the static friction limit is overcome, a partial recovery of the bristle deformation occurs and the bristle deformation instantaneously becomes:

$$\bar{s}(\alpha) = \frac{\mu_{\mathrm{d}}\, p(\alpha)}{k_{\mathrm{s}}} \tag{4}$$

At this point it is assumed that static friction takes place once again, since the normal contact pressure has not changed, while the bristle deformation has reduced; then, the bristle deforms again in elastic way, starting from the initial deformation given by Eq. 4, up to a new point where the static friction limit is overcome again. This means that the *stick–slip* phenomenon takes place.
In order to analyze the problem from a mathematical point of view, the driving and the driven pulley are described separately in the following.

Significant parameters for this model are the belt speed V_{b} and the speed of the driven pulley ω_{dn}, representing the state variables of the system which have to be determined on the basis of the equilibrium conditions of the pulleys and the congruence conditions about the tension on the tight and slack side.

In the following, in order to evaluate the deformation of the bristles, the relative slip velocity $V_{\mathrm{s},i}$ will be used for convenience (where i can indicate either the driving or the driven pulley). This is a scalar positive quantity, which can be computed on the basis of the belt speed and of the peripheral speed of the pulleys, i.e. $V_{\mathrm{s,dg}} = \omega_{\mathrm{dg}}R_{\mathrm{dg}} - V_{\mathrm{b}}$ and $V_{\mathrm{s,dn}} = V_{\mathrm{b}} - \omega_{\mathrm{dn}}R_{\mathrm{dn}}$ for the driving and driven pulley, respectively.

2.1. Contact stresses for the driving pulley

Let us consider the driving pulley. Just after the entrance into the pulley, both the bristle deformation s_{dg} and the contact stress τ_{dg} vary linearly with the angular coordinate α, until the static friction limit is overcome:

$$s_{\mathrm{dg}}(\alpha) = \int_0^{\frac{\alpha}{\omega_{dg}}} V_{\mathrm{s,dg}}\mathrm{d}t = \int_0^{\alpha} \frac{V_{\mathrm{s,dg}}}{\omega_{dg}}\mathrm{d}\tilde{\alpha} = \frac{V_{\mathrm{s,dg}}}{\omega_{\mathrm{dg}}}\alpha \tag{5}$$

$$\tau_{\mathrm{dg}}(\alpha) = k_s\, s_{\mathrm{dg}}(\alpha) = k_s \frac{V_{s,dg}}{\omega_{dg}}\alpha \tag{6}$$

At the same time the belt tension can be obtained by the following:

$$T_{\mathrm{dg}}(\alpha) = T_1 - \int_0^{\alpha} \tau_{\mathrm{dg}}(\alpha)\; R_{\mathrm{dg}}\mathrm{d}\tilde{\alpha} \tag{7}$$

Then, in the first part of the contact arc, where Eq. 5 and Eq. 6 hold, the following relationship can be obtained:

$$T_{\mathrm{dg}}(\alpha) = T_1 - \int_0^{\alpha} k_{\mathrm{s}}\; s_{\mathrm{dg}}(\alpha)\; R_{\mathrm{dg}}\mathrm{d}\tilde{\alpha} = T_1 - k_{\mathrm{s}}\frac{V_{\mathrm{s,dg}}R_{\mathrm{dg}}}{2\omega_{\mathrm{dg}}}\alpha^2 \tag{8}$$

which shows that the belt tension reduces with α according to a quadratic law, till the static friction keeps the bristle into the adhesion condition. The normal contact pressure reduces in similar way (i.e. following a quadratic law as a function of the angular coordinate α):

$$p_{\mathrm{dg}}(\alpha) = \frac{T_{\mathrm{dg}}(\alpha) - qV_{\mathrm{b}}^2}{R_{\mathrm{dg}}} = \frac{T_1 - k_s\frac{V_{\mathrm{s,dg}}R_{\mathrm{dg}}}{2\omega_{\mathrm{dg}}}\alpha^2 - qV_{\mathrm{b}}^2}{R_{\mathrm{dg}}} \tag{9}$$

The maximum tangential stress which can be transmitted by friction is given by:

$$\tau_{\mathrm{max}}(\alpha) = \mu_{\mathrm{s}}\; p_{\mathrm{dg}}(\alpha) = \mu_{\mathrm{s}}\frac{T_1}{R_{\mathrm{dg}}} - \mu_{\mathrm{s}}\frac{qV_{\mathrm{b}}^2}{R_{\mathrm{dg}}} - \mu_{\mathrm{s}}\; k_{\mathrm{s}}\frac{V_{\mathrm{s,dg}}}{2\omega_{\mathrm{dg}}}\alpha^2 \tag{10}$$

and reduces according to a quadratic law.

Considering that the tension required to keep the bristle in the adhesion condition gets higher as the angular coordinate increases (see Eq. 6), while the maximum tangential stress that can be transmitted reduces according to Eq. 10, it may happen that, for a given angular position, the belt may start to slip. This occurs at a precise angular position $\alpha_{\mathrm{s,dg}}$ along the driving pulley which can be obtained upon equating Eq. 6 and Eq. 10 :

$$\alpha_{\mathrm{s,dg}} = \frac{-\frac{k_{\mathrm{s}}V_{\mathrm{s,dg}}}{\omega_{\mathrm{dg}}} + \sqrt{\left(\frac{k_{\mathrm{s}}V_{\mathrm{s,dg}}}{\omega_{\mathrm{dg}}}\right)^2 + \frac{2\mu_{\mathrm{s}}^2 k_{\mathrm{s}}V_{\mathrm{s,dg}}}{R_{\mathrm{dg}}\omega_{\mathrm{dg}}}\left(T_1 - qV_{\mathrm{b}}^2\right)}}{\mu_{\mathrm{s}}\frac{k_{\mathrm{s}}V_{\mathrm{s,dg}}}{\omega_{\mathrm{dg}}}} \tag{11}$$

It is worth noting that this angular coordinate depends on the belt speed V_{b}; indeed, as already observed, the term $V_{\mathrm{s,dg}}$ can be expressed in terms of ω_{dg} and V_{b}, which represents the main state variable, considering the driving pulley. The belt tension

$T_{\mathrm{s,dg}}$ at the coordinate $\alpha_{\mathrm{s,dg}}$ can be obtained by substituting Eq. 11 into Eq 8.

The following Fig. 2 shows the graphical solution, obtained by the intersection of the parabola describing the maximum transmissible contact stress by static friction and the linear behavior describing the bristle tension, which increases over the angular coordinate α. The slope of the linear segments is proportional to the slip velocity according to Eq. 6; the dashed area underneath the piecewise curve describing the contact stresses is proportional to the belt tension variation over the contact arc.

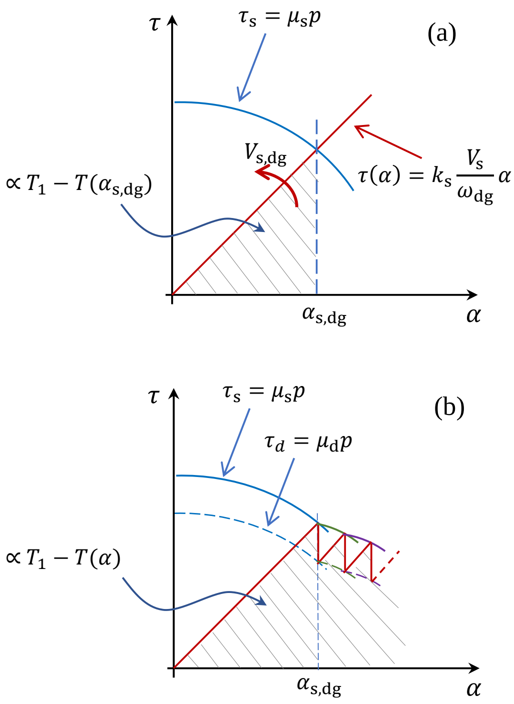

Figure 2: Maximum transmissible stress by static friction and contact stresses (a); *stick-slip* phenomenon after the adhesion arc (b). The parabolic segments represent the maximum stresses that can be transmitted by static friction and the stresses that are transmitted by dynamic friction; the red piecewise linear behavior represents the contact stress between the belt and the pulley.

If the contact pressure is relatively high (high values of belt preload) and the driving torque is relatively low, it may also happen that the friction limit is never reached and slip never takes place. In this case, the intersection between the parabola representing the maximum tangential stress and the linear trend describing the tangential stress along the contact arc, happens beyond the angular coordinate representing the contact arc.

As already stated, for $\alpha \geq \alpha_{\mathrm{s,dg}}$, the characteristic *stick–slip* phenomenon occurs, as showed in Fig. 2(*b*). In particular, the reduction of the friction coefficient from μ_{s} to μ_{d} once the friction limit is reached causes a reduction of the contact stress acting on the bristle and, consequently, a reduction of the bristle deformation which becomes:

$$\bar{s}_{\mathrm{dg}} = \frac{\mu_{\mathrm{d}} p_{\mathrm{dg}}(\alpha_{s,dg})}{k_{\mathrm{s}}} \tag{12}$$

Starting from this deformation, it is assumed that static friction occurs again, since the bristle deformation is reduced even if the contact pressure does not vary. Then, the bristle deformation increases again, proportionally to the slip velocity, as long as the contact stress is lower than the maximum value imposed by the friction limit. This kind of behaviour repeats itself several times as shown in Fig. 2b. When the friction limit has been reached for the i-th time, the bristle deformation is

$$s_{\mathrm{dg}}^{(i+1)} = \bar{s}_{\mathrm{dg}}^{(\mathrm{i})} + \frac{V_{\mathrm{s,dg}}}{\omega_{\mathrm{dg}}}\left(\alpha - \alpha_{\mathrm{s,dg}}^{(i)}\right) \tag{13}$$

It is worth noting that $\alpha_{\mathrm{s,dg}}^{(1)}$, related to the first slip event (i.e. for i=1), is the value $\alpha_{\mathrm{s,dg}}$ computed in Eq. 11, while $\bar{s}_{\mathrm{dg}}^{(i)}$ is the bristle deformation in the i-th segment, related to the friction coefficient μ_{d} and to the angular coordinate $\alpha_{\mathrm{s,dg}}^{(i)}$ (defined as in Eq. 12). The bristle deformation can then represented by a piecewise linear function as follows:

$$s_{\mathrm{dg}}(\alpha) = \begin{cases} \frac{V_{\mathrm{s,dg}}}{\omega_{\mathrm{dg}}} & \text{if} \quad 0 \leq \alpha \leq \alpha_{\mathrm{s,dg}} \\ \bar{s}_{\mathrm{dg}}^{(i)} + \frac{V_{\mathrm{s,dg}}}{\omega_{\mathrm{dg}}}\left(\alpha - \alpha_{s,dg}^{(i)}\right) & \text{if} \quad \alpha_{\mathrm{s,dg}}^{(i)} < \alpha \leq \alpha_{\mathrm{s,dg}}^{(i+1)} \end{cases} \tag{14}$$

and, consequenly, the contact stress is piece-wisely defined as well:

$$\tau_{\mathrm{dg}}(\alpha) = k_{\mathrm{s}} s_{\mathrm{dg}}(\alpha) = \begin{cases} k_{\mathrm{s}}\left(\frac{V_{\mathrm{s,dg}}}{\omega_{\mathrm{dg}}}\right) & \text{if} \quad 0 \leq \alpha \leq \alpha_{\mathrm{s,dg}} \\ k_{\mathrm{s}}\left(\bar{s}_{\mathrm{dg}}^{(i)} + \frac{V_{\mathrm{s,dg}}}{\omega_{\mathrm{dg}}}\left(\alpha - \alpha_{s,dg}^{(i)}\right)\right) & \text{if} \quad \alpha_{\mathrm{s,dg}}^{(i)} < \alpha \leq \alpha_{\mathrm{s,dg}}^{(i+1)} \end{cases} \tag{15}$$

Once the contact stress is defined along the whole winding arc, the belt tension can be obtained as:

$$T_{\mathrm{dg}}(\alpha) = T_1 - \int_0^{\alpha} \tau_{\mathrm{dg}}(\alpha)\, R_{\mathrm{dg}}\, \mathrm{d}\tilde{\alpha} = T_{\mathrm{s,dg}}^{(i)} - \int_{\alpha_{s,dg}^{(i)}}^{\alpha} \tau_{\mathrm{dg}}(\alpha)\, R_{\mathrm{dg}}\, \mathrm{d}\tilde{\alpha} = T_{\mathrm{s,dg}}^{(i)} - \int_{\alpha_{s,dg}^{(i)}}^{\alpha} R_{\mathrm{dg}} k_{\mathrm{s}} s_{\mathrm{dg}}^{(i+1)}(\alpha)\, \mathrm{d}\tilde{\alpha} \tag{16}$$

which explains that the belt tension reduces in a piecewise quadratic way, with a slower rate as the angle increases, since the contact pressure reduces (such behavior has been intentionally amplified in the schematic representation of Fig. 2b).

The tension T_2 on the slack side can be obtained as $T_{\mathrm{dg}}(\alpha_{\mathrm{dg}})$, where α_{dg} is the contact angle on the driving pulley. Then, the solution exists (i.e. the equilibrium and congruence equations for the driving pulley are satisfied), if a belt velocity V_{b} can be found such that $(T_1 - T_{\mathrm{dg}}(\alpha_{\mathrm{dg}}))\, R_{\mathrm{dg}} = M_{\mathrm{dg}}$. This is an integral problem that has to be solved in a numerical way. With reference to Fig. 2b, the solution is found when the area underneath the piecewise function describing the contact stress gives the required variation in the belt tension.

2.2. *Contact stresses for the driven pulley*

For the driven pulley similar considerations to those already made for the driving pulley hold. In this case, however, the speed of the belt is greater than the peripheral speed of the pulley and the belt tension increases along the contact angle. Equations 1–6 are still valid, as well as the general definition of the maximum transmissible stress (first part of Eq. 10) (with the due substitutions of the angular speed ω_{dn} and of the radius R_{dn} of the driven pulley); the belt tension along the contact angle is given by:

$$T_{dn}(\alpha) = T_2 + \int_0^{\alpha} \tau_{dn}(\alpha)\ R_{dn}\ d\tilde{\alpha} = T_2 + k_s \frac{V_{s,dn} R_{dn}}{2\omega_{dn}} \alpha^2 \quad (17)$$

Considering that the belt tension, and consequently the contact pressure, increases, depending on the operating conditions (applied torque) and on the belt-pulley friction characteristics, for the driven pulley the following three steady-state conditions may take place (Fig. 3):

- the belt (bristle) is in the adhesion condition throughout all the contact angle and slip never occurs (this is favored by very low torque values applied to the pulley);
- the slip condition is encountered for a given angle $\alpha_{s,dn}$ and the *stick–slip* phenomenon starts after that angle, as already described for the driving pulley;
- the slip condition is encountered and the *stick–slip* phenomenon occurs for a certain arc, after which the adhesion condition is met, again (this behavior is favored by a large difference between the static and dynamic friction coefficients).

With reference to the second and third case, the angular coordinate $\alpha_{s,dn}$ can be obtained in a similar way, as already done for the driving pulley. In this case the following relationship can be obtained:

$$\alpha_{s,dn} = \frac{-\frac{k_s V_{s,dn}}{\omega_{dn}} - \sqrt{\left(\frac{k_s V_{s,dn}}{\omega_{dn}}\right)^2 - \frac{2\mu_s^2 k_s V_{s,dn}}{R_{dn}\omega_{dn}}\left(T_2 - qV_b^2\right)}}{\mu_s \frac{k_s V_{s,dn}}{\omega_{dn}}} \quad (18)$$

As for the driving pulley, once the adhesion limit is reached, the contact stress suddenly varies due to the difference between static and dynamic friction. With reference to the regions where stick–slip occurs, for the driven pulley Eq. 14 and Eq. 15 become:

$$s_{dn}(\alpha) = \begin{cases} \frac{V_{s,dn}}{\omega_{dn}} & \text{if} \quad 0 \le \alpha \le \alpha_{s,dn} \\ \bar{s}_{dn}^{(i)} + \frac{V_{s,dn}}{\omega_{dn}}\left(\alpha - \alpha_{s,dn}^{(i)}\right) & \text{if} \quad \alpha_{s,dn}^{(i)} < \alpha \le \alpha_{s,dn}^{(i+1)} \end{cases} \quad (19)$$

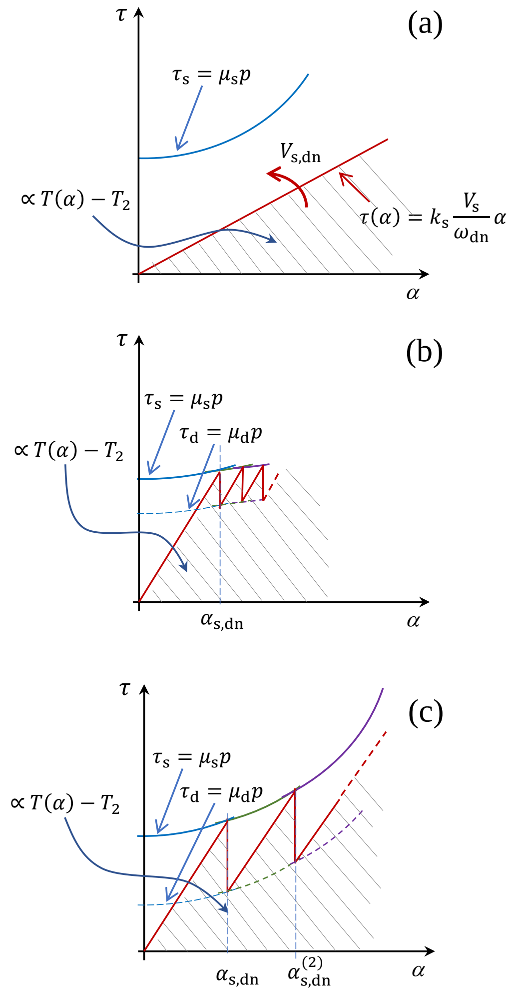

Figure 3: Contact stresses between belt and driven pulley: the friction limit is never reached in (a); the static friction limit is reached for $\alpha_{s,dn}$, beyond which *stick-slip* takes place till the exit from the pulley (b); after a contact arc where *stick-slip* occurs, a new adhesion arc is present toward the exit form the pulley (c)

$$\tau_{dn}(\alpha) = k_s s_{dn}(\alpha) = \begin{cases} k_s \left(\frac{V_{s,dn}}{\omega_{dn}}\right) & \text{if} \quad 0 \le \alpha \le \alpha_{s,dn} \\ k_s \left(\bar{s}_{dn}^{(i)} + \frac{V_{s,dn}}{\omega_{dn}}\left(\alpha - \alpha_{s,dn}^{(i)}\right)\right) & \text{if} \quad \alpha_{s,dn}^{(i)} < \alpha \le \alpha_{s,dn}^{(i+1)} \end{cases} \quad (20)$$

and the belt tension is:

$$T_{dn}(\alpha) = T_2 + \int_0^{\alpha} \tau_{dn}(\alpha)\ R_{dn}\ d\tilde{\alpha} = T_{s,dn}^{(i)} + \int_{\alpha_{s,dn}^{(i)}}^{\alpha} \tau_{dn}(\alpha)\ R_{dn}\ d\tilde{\alpha} = T_{s,dn}^{(i)} + \int_{\alpha_{s,dn}^{(i)}}^{\alpha} R_{dn} k_s s^{(i+1)}(\alpha)\ d\tilde{\alpha} \quad (21)$$

In this case, the tension T_1 on the tight side can be obtained as $T_{dn}(\alpha_{dn})$, where α_{dn} is the contact angle on the driving pulley and the solution exists (i.e. the equilibrium and congruence conditions are satisfied) if an angular velocity ω_{dn} of the driven pulley can be found such that $(T_{dn}(\alpha_{dn}) - T_2) R_{dn} = M_{dn}$. Also in this case the solution to the integral problem has to be found by a numerical routine.

3. Particular case in which $\mu_s = \mu_d$

A particular case arises if the static and dynamic friction coefficients have the same value. In this case the parabolic laws which describe the maximum tangential stress that can be transmitted by static friction and the tangential stress that are transmitted under dynamic friction conditions coincide. Then, it follows that, for the driving pulley, once the static friction limit is reached, the tangential stress change according to a single parabola (Fig. 4a). In the case of the driven pulley, in addition to such condition (Fig. 4b), it may also happen that, after a certain slipping arc, the tangential stresses due to the different relative speed between the belt and the pulley are lower than those which can be transmitted by static friction and, as a consequence, a new adhesion arc takes place (Fig. 4c). This starts from the point where the derivative of the parabolic function describing the contact stress which are transmitted by friction is equal to the slope of the linear trend describing the relationship between slip and bristle stress. This condition depends on operating parameters, such as applied torque, friction coefficient and slip.

It can be easily recognized that the creep model relationship holds in this case. Then, it can be observed that, with reference to the slip portion of the contact angle, the developed model includes, as a particular case, the classical model which is presented on classical text books.

The main difference, with respect to the classical treatment, is that for a given torque, once the belt (bristle) stiffness is assigned, the fundamental operating parameters are the belt speed V_b and the driven pulley rotating speed ω_{dn}, which allows the whole set of constitutive, equilibrium and congruence conditions to be satisfied. In the classical treatment of this subject, on the other side, once the torque and the friction coefficient are given, the slip angle (which is the same for both the pulleys), within which the belt tension varies according to an exponential law, can be directly determined, independently from the belt speed and belt constitutive properties.

4. Model implementation

The brush-model presented in this work was implemented in the Mathematica© language, in order to investigate the belt tension and the contact stresses along the contact arc and to make comparison with the creep and shear+creep models for some given transmissions.

As it usually happens in reality, a resistance torque M_{dn} was considered to be applied to the driven pulley, while the angular velocity ω_{dg} was considered to be applied to the driving pulley. The belt is subject to a given pre–load T_0 and it has to be verified if it is sufficient for the required power that has to be transmitted.

As already explained, the steady–state solution exists if a belt

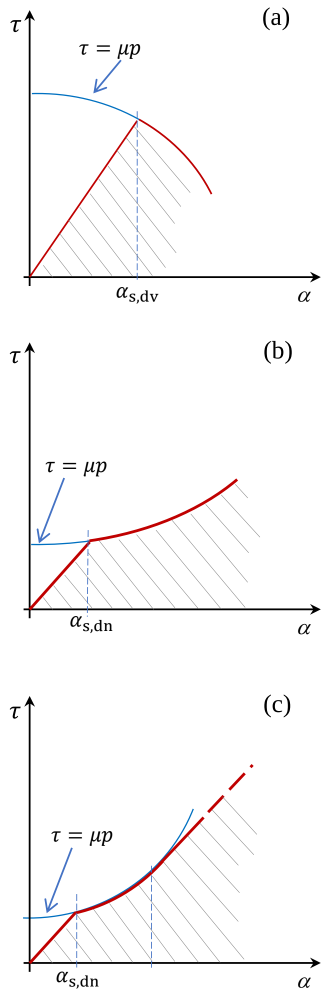

Figure 4: Contact stress between the belt and the pulley if $\mu_s = \mu_d$: driving pulley (a); driven pulley with high slip value (b); driven pulley with low slip value (c).

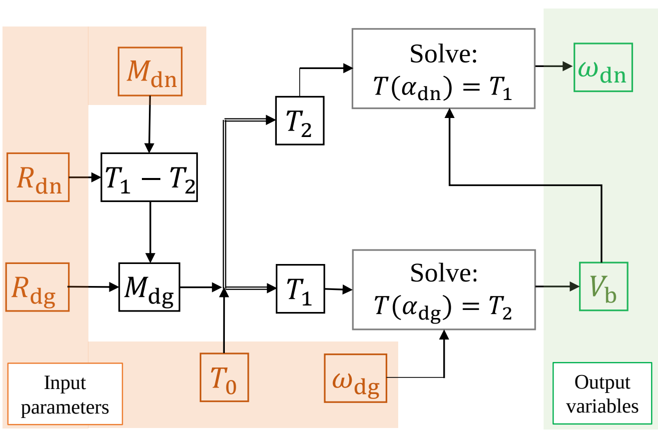

Figure 5: Schematic of the logic of the developed model.

speed V_b and a driven pulley angular speed ω_{dn} can be found, such that the required applied torques M_{dg} and M_{dn} (or the belt tension variation) are obtained.

Symbol	Parameter	Units	Value
k_s	Bristle stiffness	N/m^2	5.072 $\times 10^6$
μ_d	Dynamic friction coefficient	-	0.3
μ_s	Static friction coefficient	-	0.36
q	Belt mass per unit of length	kg/m	0.24

Table 1: Model parameters.

The logic procedure is illustrated in Fig. 5: given the resistant moment M_{dn} and the radii of the driving and driven pulleys, R_{dg} and R_{dn} respectively, it is possible to calculate, in steady-state conditions, the difference between the tension in the tight and slack side of the belt and, consequently, the driving moment M_{dg}. Given the belt pre–load T_0 the tension in the tight and slack side of the belt is then obtained.
Finally, given the driving pulley rotating speed ω_{dg}, if the solution exists, the belt speed V_b, which determines the tension variation over the driving pulley, has to be computed by solving an integral problem.

For the driven pulley, once the belt speed is known, if the solution exists, the tension variation is determined by the rotating speed ω_{dn}, which, again, has to be computed by solving an integral problem. This is illustrated in Fig. 2 and in Fig. 3, for the driving and for the driven pulley, respectively.

It is worth noting that T_0 is a parameter which has a key role for the torque transmission capability. In particular, if the solution of the integral problem does not exist for one or both the pulleys, the pre–load T_0 can be varied to search for possible solutions.

Once the torques and angular speeds of the pulleys are known, the power transmitted and, consequently, the transmission efficiency can be easily computed. The described model can therefore provide the contribution of the power losses coming from the contact stresses between the belt and the pulleys. Having assumed a purely elastic model for the bristles, it is not possible to assess the power losses due to hysteresis of the belt, although it is possible to calculate the elastic energy stored in the bristles coming out from the pulleys, which is lost and not not returned back into the system in the form of mechanical work.

5. Numerical example and discussion

The brush model described in previous sections was implemented in a general purpose program to analyze the results of the simulation, and in particular, to investigate the contribution to the transmitted torque arising from static friction and from sliding (*stick–slip*) contact. The transmission system taken as reference for the analysis is composed of driving and driven pulley, both having a 40 mm radius (the contact arc is π on both pulleys); the rotating speed ω_{dg} of the driving pulley is 300 rad/s, while the other parameters are given in Tab. 1.

Firstly, a torque that may produce slip conditions on both pulleys was looked for. To this aim Eq. 11 and 18 were solved with respect to V_b and ω_{dn}, for the case of $\alpha_{s,dg} = \alpha_{s,dg} = \pi$. By this way, the maximum torques that can be transmitted by the driving and driven pulley under adhesive contact conditions (no slip), have been determined by using equations 16 and 21: these torques resulted 6.45 Nm and 11.70 Nm for the driving and driven pulley, respectively. Therefore, in order to get some slip angle on both pulleys it is necessary to apply torque greater than 11.70 Nm.

The torque that can be transmitted in complete sliding condition was also determined for the case of the driving pulley, considering $V_b = 0$ and this resulted 14.05 Nm.

Simulations were then carried out with a moment of 12.5 Nm, in order to have both adhesion and sliding conditions on both pulleys.

Figure 6 gives the contact stresses on both the driving and the driven pulley. Different arcs of adhesion were obtained for the driving and the driven pulley. In particular, for the driving pulley $\alpha_{s,dg} \approx 0.8$ rad, where the static friction limit is reached for the first time. For the driven pulley, that happens for $\alpha_{s,dn} \approx 1$ rad. Beyond these angles *stick–slip* takes places on both pulleys.

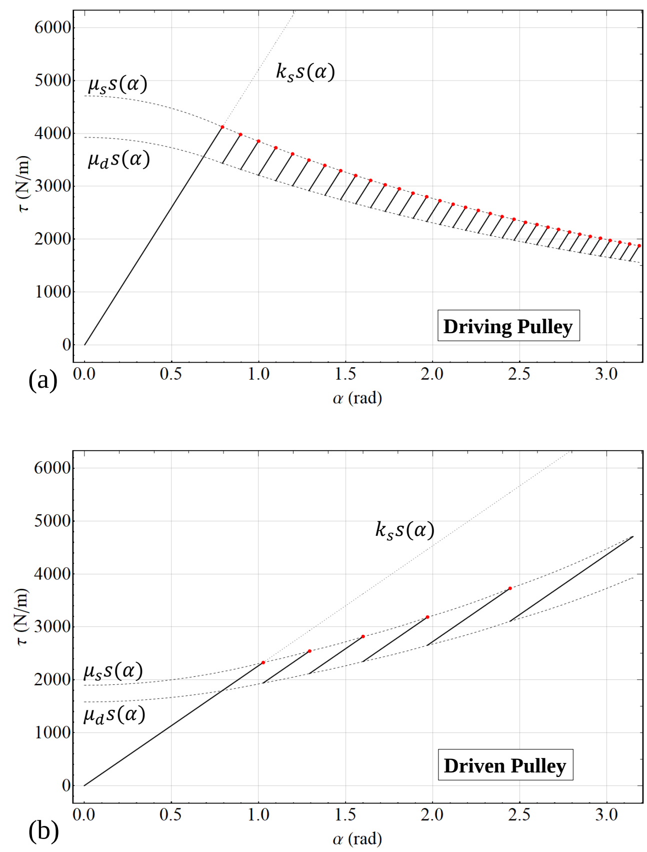

Figure 6: Contact stress along the winding arc for the driving (a) and driven pulley (b).

It is worth noting that the friction limit is reached many times for the driving pulley, while this happens only few times for the driven pulley; this is a consequence of the fact that the contact pressure decreases along the contact arc for the driving pulley, while it increases for the driven pulley. In particular, with reference to the driven pulley, it can be observed in Fig. 6 that after the static friction limit is reached for the fifth time ($\alpha \approx 2.45$ rad), the bristle starts to deform elastically and the friction limit is no more encountered till the exit from the pulley; this corresponds to the case shown in Fig. 3c.

Figure 7 shows the bristle deformation along the contact arc for both the driving and the driven pulley. The contributions of the elastic deformation and of the slip, taking place every time the friction limit is reached, are given. The slip contribution varies at discrete increments, given by $\frac{(\mu_s-\mu_d)\,p(\alpha)}{k_s}$. For the driving pulley, the total deformation is greater and the friction limit is reached at a smaller angle, i.e. $\alpha_{s,dg} \leq \alpha_{s,dn}$.

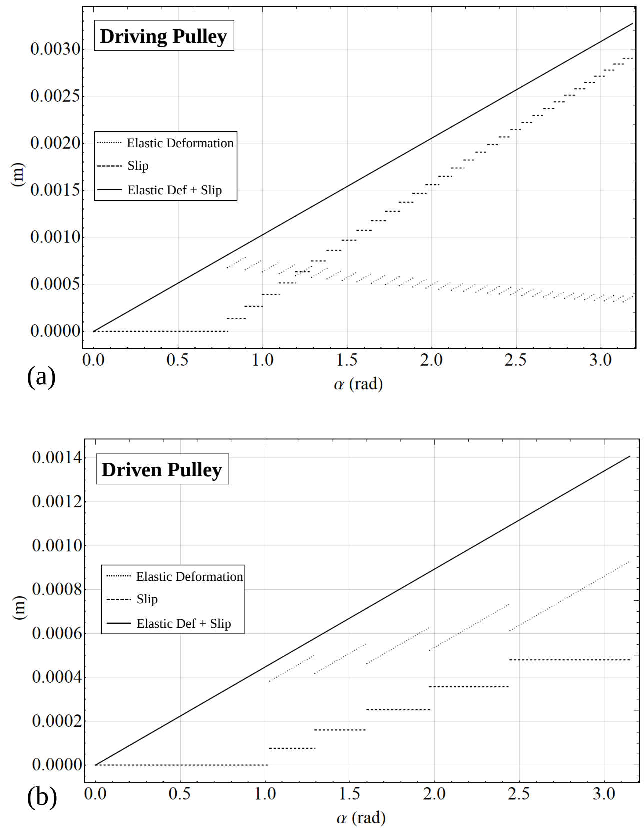

Figure 7: Bristle elastic deformation and slip along the winding arc for the driving and driven pulley.

Due to the variation of the contact pressure, it can be observed that the elastic deformation reduces along the contact arc in the driving pulley, while it gets greater along the contact arc of the driven pulley. In a similar way, the slip deformation increments, get smaller and smaller over the contact angle in the driving pulley, while they increase progressively for the driven pulley. In addition, the discrete slips extension reduces with the angular coordinate α for the driving pulley, while these increase for the driven pulley, since the contact pressure rises along the driven pulley winding arc.

Figure 8 shows the belt tension variation over the contact angle, as obtained by the brush model, in comparison to the previsions of the creep and the shear+creep models. In the figure, the transition angle from adhesion conditions to slip (*stick–slip*) is marked by a vertical line, for each one of the considered models. As it can be observed, the main difference is in the prevision of the sliding angle, which according to the classical creep model is the same for the driving and the driven pulley and results much larger than the sliding angle that can be determined by the shear+creep model or the brush model. Smaller differences can be observed between the angle obtained in the present work and the one obtained by the shear+creep model, where the speed difference between the pulley and the belt is not explicitly considered.

A similar approach to the one described in this work was fol-

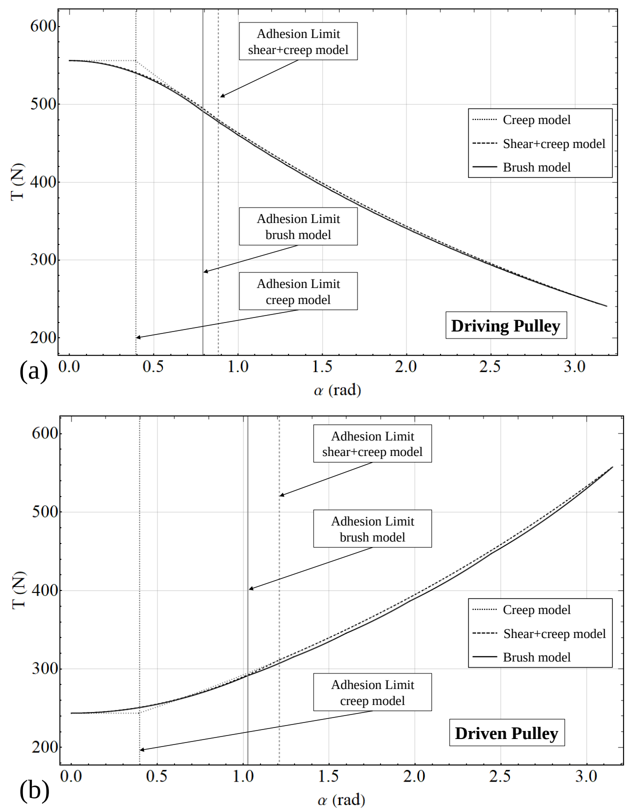

Figure 8: Adhesion boundaries for different models and belt tension along the winding arc of the driving (a) and driven pulley (b).

lowed by *Kong* and *Parker* in [11], for the case of an elastic belt. In that work the angular deformation is considered as in the shear+creep model, even if the *stick–slip* phenomenon (which has been documented in the experimental work of *Della Pietra, Timpone* [12]) is not taken into account .

The following Fig. 9 shows the torque transmitted along the contact angle according to the present model, the *Firbank*'s model (shear + creep) and the *Grashof*'s model (creep). It is evident that the whole contact angle contributes to the transmitted torque, as also documented in [12]–[13]. On the contrary, according to the classic theory, only the slip arc is responsible for the torque transmission.

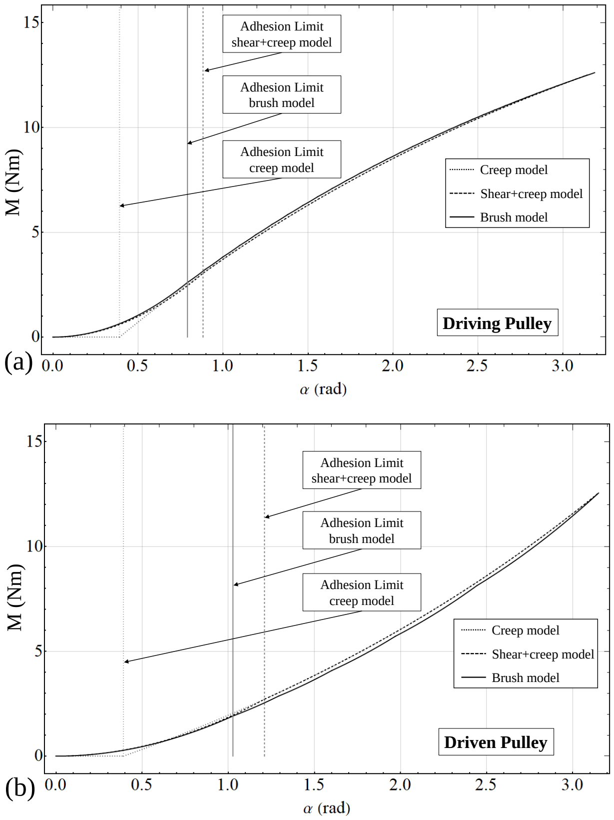

Figure 9: Torque transmission contribution along the winding arc of the driving (a) and driven pulley (b).

6. Transmission efficiency

Through the developed model it is possible to evaluate the transmission efficiency in two independent ways: by considering the ratio of the output to input torque, or by evaluating the power losses due to slip and to the deformation of the bristles (elastic potential energy).

In the former case, the efficiency can be simply obtained by the following relationship:

$$\eta = \frac{M_{\rm dn}\omega_{\rm dn}}{M_{\rm dg}\omega_{\rm dg}} \tag{22}$$

where, for the analyzed case for which $M_{\rm dg} = M_{\rm dn}$ (equal radius of the pulleys), the efficiency is obtained by the ratio of the driven pulley rotational speed to the driving pulley rotational speed.

In the latter case, the following relationships, $D_{\rm dg}$ and $D_{\rm dn}$, give the energy dissipated by friction, for the driving and driven pulley, respectively:

$$D_{\rm dg} = \sum_{i=1}^{N} T(\alpha^i_{\rm dg})(s^i_{\rm dg}(\alpha^i_{\rm dg}) - s^{i+1}_{\rm dg}(\alpha^i_{\rm dg})) \tag{23}$$

$$D_{\rm dn} = \sum_{i=1}^{N} T(\alpha^i_{\rm dn})(s^i_{\rm dn}(\alpha^i_{\rm dn}) - s^{i+1}_{\rm dn}(\alpha^i_{\rm dn})) \tag{24}$$

where $\alpha^i_{\rm dg}$ and $\alpha^i_{\rm dn}$ represent the angle on the driving or driven pulley where the friction limit is reached for the i−th time, while $s^i_{\rm s,dg}$ and $s^i_{\rm s,dn}$ represent the bristle slip relative to the driving and driven pulley, which takes place at angular position $\alpha^i_{\rm dg}$ and $\alpha^i_{\rm dn}$.

The terms $U_{\rm dg}$ and $U_{\rm dn}$ give the elastic potential energy stored in the bristle:

$$U_{\rm dg} = \frac{1}{2} k_s\, s^2_{\rm dg}(\pi)\,\pi\, R_{\rm dg} \tag{25}$$

$$U_{\rm dn} = \frac{1}{2} k_s\, s^2_{\rm dn}(\pi)\,\pi\, R_{\rm dn} \tag{26}$$

In the previous equations $s_{\rm dg}$ and $s_{\rm dn}$ are the elastic deformation of the bristle at the exit from the driving and driven pulley. It is worth noting that this energy is not turned back into the system and, having neglected any damping contribution, is lost as vibration energy of the bristle at the exit from the pulleys.

By using previous relationships, the transmission efficiency can be evaluated by the following:

$$\eta = \frac{M_{\rm dg}\alpha_{\rm dg} - (D_{\rm dg} + D_{\rm dn} + U_{\rm dg} + U_{\rm dn})}{M_{dg}\alpha_{\rm dg}} = 1 - \frac{D_{\rm dg} + D_{\rm dn} + U_{\rm dg} + U_{\rm dn}}{M_{\rm dg}\alpha_{\rm dg}} \tag{27}$$

The numerical model was used to obtain an estimate of the efficiency and to evaluate the power losses, highlighting the contribution of the driving and driven pulley for different values of the transmitted torque.

Table 2 shows the efficiency obtained by Eq. 22 and by Eq. 27 for different values of the transmitted torques which produce both adhesion and *stick-slip* on both pulleys. It can be observed that the transmission efficiency reduces as the torque increases and how the efficiencies obtained on the basis of the power transmitted by the pulleys or on the basis of the energy losses (friction sliding and elastic potential energy) are in very good mutual agreement.

Figure 10 shows the transmission efficiency as a function of the applied torque. Three different regions can be distinguished in the plot:

- in the first region, for low values of the applied torque,i.e. $0 \leq M \leq 6.45$ Nm, only elastic deformation is present on both the pulleys (no slip); in this region the efficiency reduces linearly as the torque increrases;

M (Nm)	η (Eq. 22)	η (Eq. 27)
12.00	97.2 %	97.1 %
12.50	96.4 %	96.4 %
13.00	94.7 %	94.7 %
13.25	93.1 %	93.2 %
13.50	92.0 %	92.2 %
13.75	89.8 %	90.2 %

Table 2: Transmission efficiency for different torque values.

- in the second region, for $6.45 \leq M \leq 11.70$ Nm, both elastic deformation and slip occur on the driving pulley, while on the driven pulley the friction limit is not reached and only elastic deformation takes place; in this region the efficiency progressively reduces with the torque;
- finally, in the third region, for $11.70 \leq M \leq 14.05$, both elastic deformation and slip occur on both pulleys; this causes a significant increment in the negative slope describing the efficiency reduction for any increment in the transmitted torque.

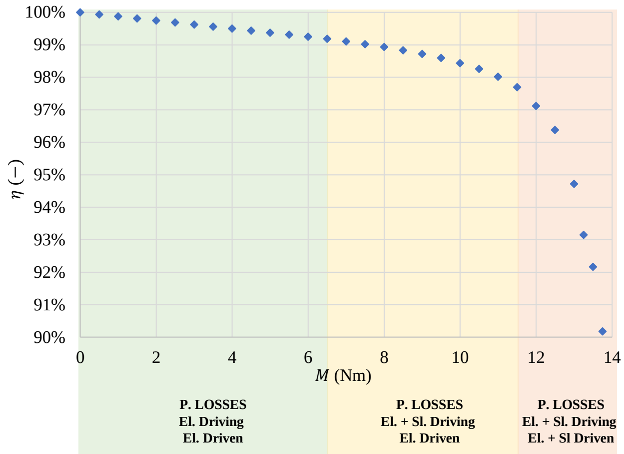

Figure 10: Transmission efficiency vs. transmitted torque.

Figure 11 shows the contribution to the power losses coming from the driving and from the driven pulley; it is interesting to observe that in the first region, as long as the belt is in adhesion condition and there is just elastic deformation with no slip in both pulleys, the power losses are equally distributed among the pulleys. In the second region, the power losses have a greater contribution (up to about 70%) from the driving pulley where slip occurs in addition to the elastic deformation. Finally, in the third region there is an oscillating behavior with approximately 65% – 72% of the power losses coming from the driving pulley where the slip contribution is greater.

Figure 12 shows the elastic potential energy contribution to the power losses for both pulleys. In the figure, it can be observed that for low values of the transmitted torque, the power losses comes entirely form the elastic deformation. Then, for intermediate torques, the elastic contribution to the power losses decreases in the driving pulley where some slip takes place, while in the driven pulley the power losses remain associated to the elastic deformation. In the third region, for higher torques, there is a significant decrement of the elastic contribution to the power losses also in the driven pulley. The power losses due to the elastic contribution tend toward zero nearby the maximum value of the torque that can be transmitted, when slip takes place almost over the whole contact arc on both pulleys.

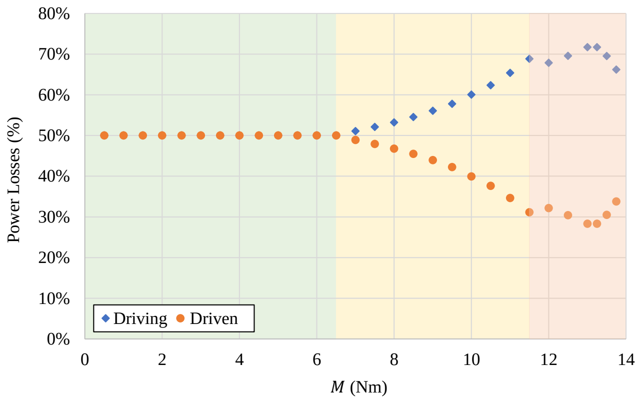

Figure 11: Percentage of power losses distribution among driving and driven pulley vs. transmitted torque.

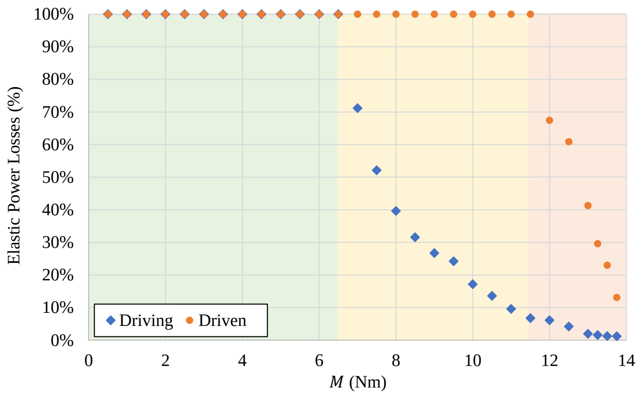

Figure 12: Percentage of the elastic power losses, with respect to the total power losses on the driving and driven pulley.

7. Conclusions

In this work, a physically based brush model, usually used for pneumatic tires, was developed and implemented to analyse the behavior of flat belts with reinforcing fibers. The belt was modeled considering an axially inextensible tension member, which the bristles constituting the matrix are connected to and purely elastic deformable bristles, while a coulomb friction model allowed the *stick–slip* phenomenon to be accounted for.

The mechanical problem was formulated so that the main state variables to be determined are the belt speed and the driven pulley rotational speed, while the rotational speed of the driving

pulley and the resistant torque are considered as input parameters; at the same time, the belt pre-load is an operating parameter to be set to look for possible existing solutions.
The solution of the constitutive congruence and equilibrium conditions, if one exists (oppositely to the classical treatment and according to what it can be reasonably expected, the solution depends on the constitutive properties of the belt material and on the belt speed), gives a detailed knowledge of the contact stresses along the winding arc, starting from which all the representative parameters can be computed, such as the portions of the adhesion and slip arcs on the driving and driven pulley and the power loss due to the contact stresses and to the elastic deformation of the belt.

The results obtained for a reference case were compared to those provided by two classical models usually used for belts: the creep model (i.e. *Euler/Grashof* model) and the shear and creep model (i.e. *Firbank model*).
Compared to the creep model, the differences are evident because, oppositely to what envisaged by the creep model, on the basis of the brush model the torque is transmitted throughout the whole contact arc. The results are, instead, more similar to those of the shear and creep model, even if the extension of the arc where elastic deformation of the bristles (shear) occurs is obtained in closed form, in relation to the physical properties of the belt (stiffness of the bristle) and to state variables, that are the belt speed and the rotating speed of the driven pulley.
Considering the region of the winding arc where stick-slip takes place, the brush model is able to foresee the *stick–slip* phenomenon which has been observed in some experimental work and which has not been considered in any theoretical model.
It is also worth noting that according to the presented model adhesion of the belt near the exit from the driven pulley may take place, after a given extension arc where slip occurs, due to the increase in the contact pressure as the belt winding arc increases.

An analysis of the transmission efficiency allowed to observe that the power losses increase suddenly as the torque gets over the value at which slip begins and to find out that the main contribution to the power losses comes from the driving pulley as soon as a slip region is present on the contact arc.

An experimental validation regarding both the belt tension and the transmission efficiency is planned to validate the results of the brush model.

References

[1] S.E. Bechtel, Vohra S., Jacob K. I., and Carlson C.D. The stretching and slipping of belts and fibers on pulleys. *Journal of Applied mechanic*, 1(67):197–20, 2000.

[2] D. G. Alciatore and Traver A. E. Multipulley belt drive mechanics: creep theory vs shear theorys. *Journal of Mechanical Design*, 4(117):506–511, 1995.

[3] Kong L. and Parker R. G. Mechanics of serpentine belt drives with tensioner assemblies and belt bending stiffness. *Journal of Mechanical Design*, 5(127):957–96, 2005.

[4] Rubin M. B. An exact solution for steady motion of an extensible belt in multipulley belt drive systems. *Journal of Mechanical Design*, 3(122):311–316, 2000.

[5] Gerber G. Belt slip – a unified approach. *Journal of Mechanical Design*, 3(118):432–438, 1996.

[6] Kong L. and Parker R. G. Mechanics and sliding friction in belt drives with pulley grooves. *Journal of Mechanical Design*, 2(128):494–502, 2006.

[7] Leamy M. J. and Wasfy T. M. Analysis of belt-driven mechanics using a creep-rate-dependent friction law. *Transactions of the American Society of Mechanical Engineers Journal of Applied Mechanics*, 6(69):763–771, 2002.

[8] Firbank T. C. Mechanics of the belt drive. *International Journal of Mechanical Sciences*, 12(12):1053–1063, 1970.

[9] Tonoli A., Amati, and Zenerino E. Dynamic modeling of belt drive systems: effects of the shear deformations. *Journal of vibration and acoustics*, 5(128):555–567, 2006.

[10] Childs T. H. C. and Parker I. K. Power transmission by flat, v and timing belts. *Tribology Series*, (14):133–142, 1989.

[11] Kong L. and Parker R. G. Microslip friction in flat belt drives. *Proceedings of the Institution of Mechanical Engineers, Part C: Journal of Mechanical Engineering Science*, 10(219):1097–1106, 2005.

[12] Della Pietra L. and Timpone F. Tension in a flat belt transmission: experimental investigation. *Mechanism and Machine Theory*, (70):129–156, 2013.

[13] Kim H., Marshek K., and Naji M. Forces between an abrasive belt and pulley. *Mechanism and Machine Theory*, 1(22):97–103, 1987.

[14] Bernard J. E., Segel L., and Wild R. E. Tire shear force generation during combined steering and braking maneuvers. *SAE Technical Paper*, page 770852, 1977.

[15] Pacejka H. B. and Sharp R. S. Shear force development by pneumatic tyres in steady state conditions: a review of modelling aspects. *Vehicle System Dynamics*, 3–4(20):121–175, 1991.

[16] Bertini L., Carmignani L., and Frendo F. Analytical model for the power losses in rubber v-belt continuously variable transmission (cvt). *Mechanism and Machine Theory*, (78):289–306, 2014.